Realistic Stochastic Virtual Microstructure Generation for Woven Fabrics and Textile Composites: The Thermal Growth Approach

Gaurav Nilakantan

Teledyne Scientific & Imaging, Thousand Oaks, CA 91360, USA

Abstract

Generating realistic 3D yarn-level finite element models of textile weaves and impregnated textile composites poses a challenge because of the complexity of the 3D architecture and the need for achieving high quality finite elements and non-intersecting yarn volumes. A common approach is to sweep a constant yarn cross-sectional shape along a smooth and continuous centerline that repeats over a unit cell length. This approach breaks down with tight and complex weave architectures. Moreover, actual microstructures of dry fabrics and textile composites are often aperiodic and non-deterministic. In this work, a new method to generate realistic virtual microstructures of woven fabrics and textile composites using a "thermal growth" approach is presented. This involves a series of mechanics-driven orthotropic volumetric expansions and shrinkages of the yarn cross-sections and centerlines that are artificially induced by prescribed thermal loads, along with mechanics-driven yarn deformations in order to "grow" or "form" the yarns into their final realistic configurations within the weave. Contact-pairs are defined between interlacing yarn surfaces to prevent yarn inter-penetrations. The final virtual microstructures are generated through a series of finite element simulations executed using LS-DYNA®. This process is demonstrated by considering the case study of a plain-weave Kevlar fabric (Style 706) used in body armor. A movie of the thermal growth process in action is available through the YouTube URL provided. The virtual microstructures are characterized using ImageJ-based image analysis and then validated against experimental microstructures. Relatively fine microstructural features are accurately reproduced. The process is amenable to any textile weave architecture including 2D, 2.5D, and 3D woven, braided, and knit architectures.

Introduction

There are several available academic and commercial codes that are capable of generating yarn-level geometric models and/or meshes of 2D and 3D woven fabrics, braids, and knits. Some codes additionally compute the effective orthotropic elastic and thermal properties of the textile composite model using various analytical (e.g. micromechanics) and hybrid-FEA techniques. Well-known examples of such codes include TexGen [1], WiseTex [2], Digital Fabric Mechanics Analyzer (DFMA) [3], Virtual Textile Morphology Suite (VTMS) [4], pcGINA [5], and mmTexLam [6]. In this paper, an innovative method of generating realistic deterministic and stochastic virtual microstructures of dry fabrics and textile composites using a "thermal growth" technique is presented, wherein a series of controlled mechanics-driven orthotropic volumetric expansions and contractions of the yarn cross-sections and yarn centerlines coupled with mechanics-driven yarn deformations are used to generate 2D, 2.5D, and 3D weave architectures. The output is a high-quality, ready-to-use finite element mesh of the textile weave with each yarn individually modeled in 3D. The framework is implemented as a series of thermostructural simulations executed using LS-DYNA. The case study of a plain-weave Kevlar fabric (Style 706) used in body armor is considered. The virtual microstructures of the finite element model are extensively validated against experimental microstructures obtained from optical microscopy characterization and ImageJ-based image analysis of the material specimens. Aside from dry fabrics, the thermal growth approach described herein can also be applied to impregnated textile composites, in which case the matrix volume mesh is also subjected to controlled volumetric expansions and contractions. For an additional case study with an angle-interlock C/SiC ceramic matrix composite, the reader is referred to Nilakantan et al. [7].

Methodology: Thermal Growth

A common approach to generating textile architectures relies on sweeping a constant yarn cross-section along a centerline trajectory. The centerline trajectories of a plain-weave fabric can be approximated by sinusoidal functions as shown in Equations (1-2).

$$y_i^{warp} = \frac{t^{warp}}{2}\cos\left(\frac{\pi x_i^{warp}}{s^{fill}}\right) \tag{1}$$

$$y_i^{fill} = \frac{t^{fill}}{2}\cos\left(\frac{\pi z_i^{fill}}{s^{warp}}\right) \tag{2}$$

here '*t*' represents the yarn thickness and '*s*' represents the yarn span. The warp yarn centerlines are along the X axis and the fill yarn centerlines along the Z axis. The Y axis represents the fabric thickness direction. Equations (1) and (2) indicate that the warp yarn cross-sectional shapes are governed by the fill yarn centerlines and vice-versa. This approach will result in what we will subsequently refer to as an "*Idealized*" virtual microstructure. In addition, we will generate a "*Realistic*" virtual microstructure using the thermal growth method and compare both approaches against the experimental material microstructure. For the thermal growth method, we begin with modeling 2D yarn cross-sections that closely represent the actual yarn size and shape directly obtained from 2D optical microscopy as shown in Figure (1). Thus, the warp yarn cross-sections were generated to be sinusoidal in shape (see Figure 1a) while those of the fill yarn cross-sections were generated to be elliptical in shape (see Figure 1b). These cross-sections are then swept along the sinusoidal centerline trajectories (see Equations 1-2) to generate the 3D yarn mesh. At this point, the finite element weave model will most likely contain unwanted yarn inter-penetrations as well as unwanted gaps between regions of a yarn's cross-section and the interlacing yarn's centerline, as schematically shown in Figure (1) for the Kevlar S706 fabric. In addition to the undesirable yarn inter-penetrations and gaps, there are various other discrepancies between the starting virtual microstructure and the actual material microstructure. These discrepancies, discussed later, will also be handled (i.e. remediated) by the thermal growth process, resulting in the final (i.e. desired) virtual microstructure also shown in Figure (1).

(a)

(b)
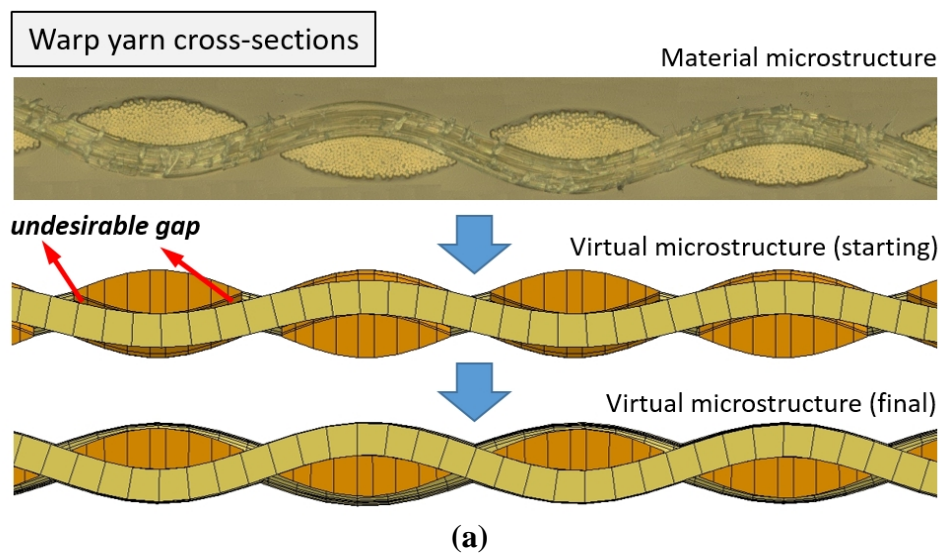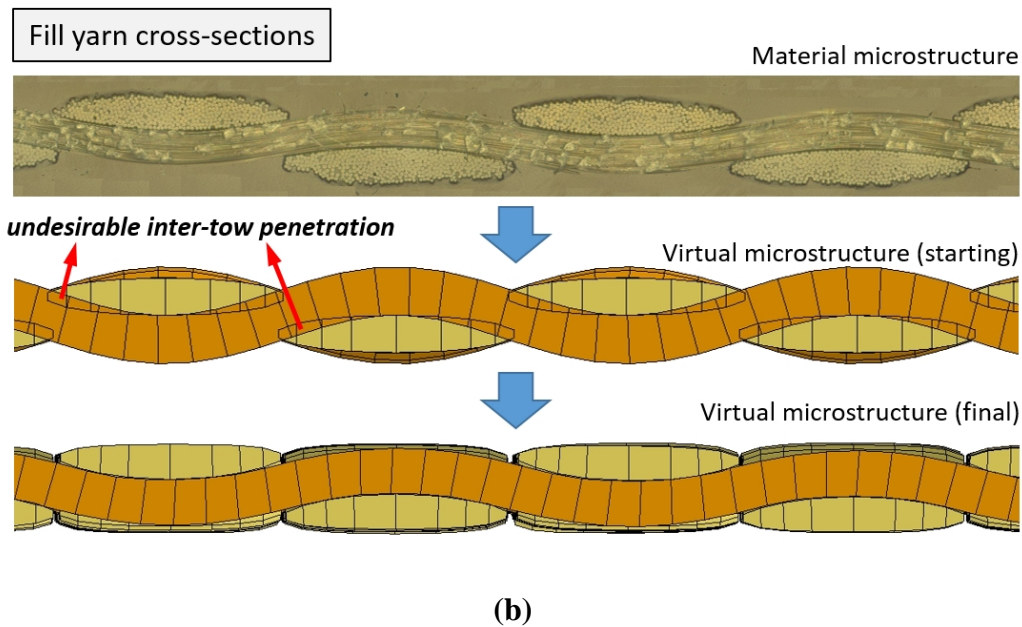
Figure 1. Kevlar S706 fabric microstructure, starting and final virtual microstructures
(a) Warp yarn cross-sections (b) Fill yarn cross-sections

The next step in the virtual microstructure generation framework involves remediating these yarn penetrations, gaps, and various other microstructural discrepancies, and 'driving' or 'forming' the yarn cross-sectional shapes, cross-sectional dimensions, and yarn centerlines into their final configuration. This process occurs in a series of steps, wherein each step represents a thermostructural simulation executed in LS-DYNA. The warp and fill yarns are assigned to an orthotropic thermoelastic material model, wherein the material properties are defined along the three yarn local material axes: *aa*, *bb*, and *cc*. The aa- axis follows the undulating yarn centerline and represents the longitudinal yarn properties, while the bb- and cc- axes represent the transverse yarn properties. A set of three Young's moduli (E_{ii}), three shear moduli (G_{ij}), three Poisson ratios (v_{ij}), and three coefficients of thermal expansion or CTE (α_{ij}) are specified separately for the warp and fill yarns. Equation (3) lists the yarn material model stress (σ)-strain (ε) relationship in the compliance form. Equation (4) lists the relationship between the thermal strains (ε^T), the CTE values (α_{ij}), and the prescribed thermal load (ΔT). Because the reference temperature is assumed to be zero, ΔT just represents the prescribed nodal temperatures. This thermal load when applied to the entire model (i.e. prescribed nodal temperatures), results in a corresponding volumetric expansion or contraction of the yarns depending on the magnitude and sign of the chosen CTE values and the prescribed thermal load. Thus, this method is referred to as the "*thermal growth*" method of generating realistic virtual microstructures. By using a locally orthotropic material model, the user can strategically manipulate the growth of the yarns separately along the three local material axes. Recall in addition to volumetric expansions and shrinkages of the yarn cross-sections and centerlines, the yarns can also mechanically deform, resulting in both mechanical and thermal strains. For example, one set of yarns may be prescribed as rigid (i.e. no change in size and shape) during one of the simulation steps, forcing a constrained growth of the orthogonal interlacing yarns against these rigid yarns and possibly also against a fixed surrounding or encapsulating surface. Another example is when the various yarns are prescribed different magnitudes of stiffness resulting in the preferential deformation of one set of yarns over the other.

$$\begin{bmatrix} \varepsilon_{11} \\ \varepsilon_{22} \\ \varepsilon_{33} \\ \varepsilon_{12} \\ \varepsilon_{13} \\ \varepsilon_{23} \end{bmatrix} = \begin{bmatrix} \dfrac{1}{E_{11}} & \dfrac{-v_{21}}{E_{22}} & \dfrac{-v_{31}}{E_{33}} & 0 & 0 & 0 \\ \dfrac{-v_{12}}{E_{11}} & \dfrac{1}{E_{22}} & \dfrac{-v_{32}}{E_{33}} & 0 & 0 & 0 \\ \dfrac{-v_{13}}{E_{11}} & \dfrac{-v_{23}}{E_{22}} & \dfrac{1}{E_{33}} & 0 & 0 & 0 \\ 0 & 0 & 0 & \dfrac{1}{2G_{12}} & 0 & 0 \\ 0 & 0 & 0 & 0 & \dfrac{1}{2G_{13}} & 0 \\ 0 & 0 & 0 & 0 & 0 & \dfrac{1}{2G_{23}} \end{bmatrix} \begin{bmatrix} \sigma_{11} \\ \sigma_{22} \\ \sigma_{33} \\ \sigma_{12} \\ \sigma_{13} \\ \sigma_{23} \end{bmatrix} + \begin{bmatrix} \varepsilon_{11}^{T} \\ \varepsilon_{22}^{T} \\ \varepsilon_{33}^{T} \\ 0 \\ 0 \\ 0 \end{bmatrix} \qquad (3)$$

$$\begin{bmatrix} \varepsilon_{11}^{T} \\ \varepsilon_{22}^{T} \\ \varepsilon_{33}^{T} \end{bmatrix} = \begin{bmatrix} \alpha_{11} & 0 & 0 \\ 0 & \alpha_{22} & 0 \\ 0 & 0 & \alpha_{33} \end{bmatrix} \begin{bmatrix} \Delta T \\ \Delta T \\ \Delta T \end{bmatrix} \qquad (4)$$

To get from the starting microstructure to the final microstructure shown in Figure (1) for the Kevlar S706 fabric, a set of eight simulations steps were run as follows. Note that these only represent one possible set of simulation steps and that the final microstructure could have been attained through other paths.

Step 1. Warp and fill cross-section shrinking
Step 2. Warp centerline shrinking
Step 3. Warp and fill cross-section shrinking
Step 4. Warp and fill cross-section expansion
Step 5. Centerline crimp interchange (warps shrink, fills expand)
Step 6. Warp yarn width expansion
Step 7. Warp centerline shrinking
Step 8. Fill yarn width expansion

A movie of the thermal growth process in action for the Kevlar S706 fabric using these eight steps can be seen in the following YouTube URL: *https://www.youtube.com/watch?v=FEZfOlU-_wQ&*. Figure (2) displays exemplary snapshots (A-E) of the thermal growth process during the eight steps. The first underlying idea behind the thermal growth framework is to initially shrink the yarn cross-sections till there is a clearly visible gap (i.e. empty space) between all the yarn volumes (e.g. see snapshot B) that had initial inter-penetrations between them (e.g. see snapshot A), and then to thermally grow them all back in size while utilizing contact definitions (e.g. node-to-surface and surface-to-surface contact algorithms [8]) between yarn surfaces to prevent them from penetrating each other (e.g. see snapshot C). When possible, another alternative is to simply start off with much smaller or scaled-down 2D yarn cross-sections, as long as they can be swept along the 1D centerlines without preprocessing errors. The second underlying idea behind the thermal growth framework is to strategically grow the various dimensions of the yarns into their final intended sizes and shapes (e.g. see snapshot E), which can occur either sequentially or simultaneously, either individually or collectively, and by using a combination of various CTE (α_{ii}) and stiffness (E_{ii}) values. By starting off with 2D yarn cross-sections that already well approximate the actual yarn cross-sectional sizes and shapes from optical micrographs of the material specimen, it becomes easier to grow the yarns into their final configurations using simple linear

orthotropic thermoelastic yarn material models. However for weaves and processing routes that result in yarn cross-sections that deviate from the typical sinusoidal and elliptical shapes (e.g. flattened, sheared, or sharp yarn cross-sections), there is a greater emphasis on the role of the yarn material model, such as non-linear orthotropic thermo-elastic-plastic material models in order to grow and deform the yarn cross-sectional shapes into their final intended configurations. For example, once the yarns enter the plastic regime of an elastic-plastic material model, they can 'flow' or be plastically squeezed during thermal growth into their final deformed configuration. For these cases, care must be taken to choose an appropriate 3D finite element formulation, mesh size, material axis update option, and hourglass formulation.
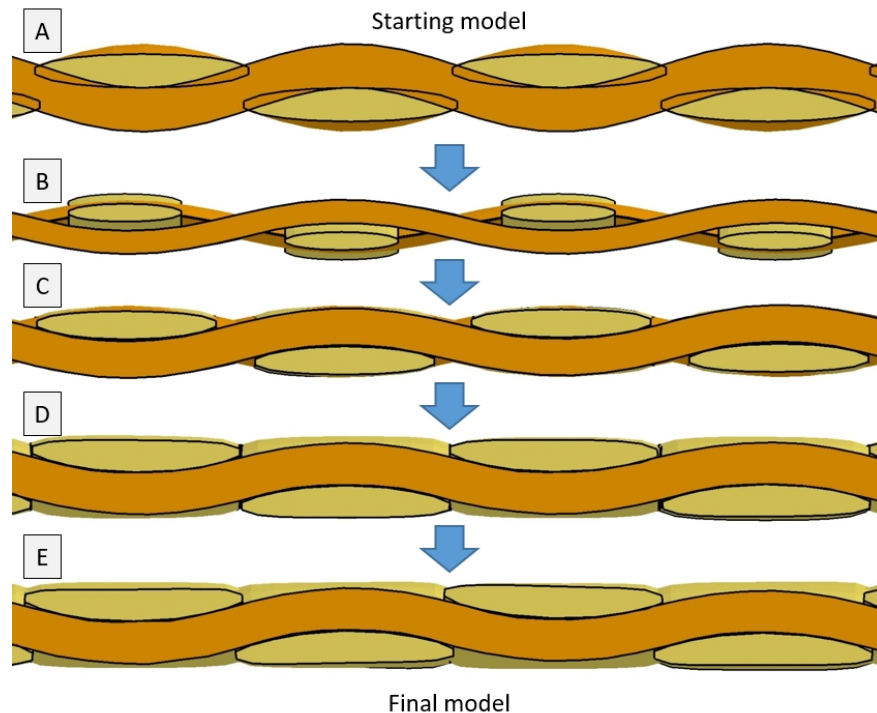
Figure 2. Exemplary snapshots (A-E) of the fill yarn cross-sections and warp yarn centerlines during the thermal growth process for Kevlar S706

The finite element mesh at the end of the thermal growth simulation runs (i.e. once the desired virtual microstructure has been obtained) is exported into a new input deck (e.g. LS-DYNA *.k* inputfile) which is now ready to be run in a new analysis. Obviously, this mesh could also be exported into other solver formats (e.g. Abaqus *.inp* inputfile). During the thermal growth simulation runs, parameters such as the fiber volume fraction (as well as the fiber packing fraction) and the local material axes (i.e. direction cosines of the aa-, bb-, cc- axes) for each solid element in the yarns should be continuously tracked, in order to impart the correct constitutive material properties and material directionality to the final exported model. This is especially important if the yarn cross-sectional area or shape changes along the length of the yarn during the thermal growth runs. Recall that in the starting virtual microstructure, the yarn cross-sectional area remains constant along the entire yarn length. In actual weave architectures, the yarn cross-sectional shape can change along the yarn length, which physically manifests itself as the individual fibers either loosely spreading apart at certain regions or getting compressively bunched up together at certain regions along the yarn length. The various parameters of interest can be dynamically stored element-by-element as history variables (e.g. HSVS) of a user-defined material model (UMAT) and then written out at the end of the simulation. During the thermal growth simulation runs, in the unlikely event that some yarn elements become very small in size or the mesh becomes excessively deformed, or it is simply desired to change the mesh density, then one option is to convert the 3D yarn mesh

back into 3D yarn volumes which is a relatively straightforward process in commercial finite element preprocessors (e.g. Altair Hypermesh®). These 3D yarn volumes can then be remeshed with hex- or tet-elements of the desired quality. However, it may now become non-trivial to specify the correct element-by-element local material axes (this information is lost during the re-meshing process) and to enforce the condition that the yarn local longitudinal direction follows the undulating yarn centerline. To resolve this issue, 1D yarn centerlines discretized with 1D elements (e.g. truss, beam) are embedded within the 3D yarns of the finite element weave model as shown in Figure (3).
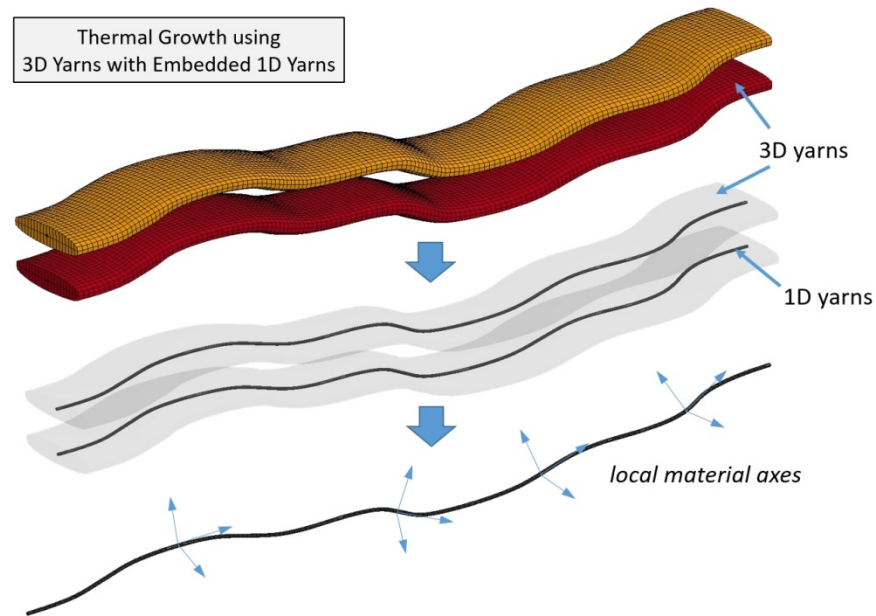
Figure 3. Tracking of local material axes during the thermal growth of 3D yarns with embedded 1D yarns

This can be done either by merging the nodes of the 1D centerline elements with the 3D yarn solid elements or by using master-slave coupling constraints (e.g. the Binary Model [9]) and then assigning a negligible stiffness to the 1D elements. This will cause the 1D centerlines to follow the deformation of the 3D yarns during the thermal growth process. Once the intended virtual microstructure has been obtained, the deformed 1D yarns can then be used with a separate script (e.g. Matlab®, Python®) to assign the element-by-element local material axes (i.e. aa, bb, cc) to each solid element. This requires looping through each of the yarn's solid elements and identifying the nearest embedded 1D element. The solid element's aa- axis (i.e. local longitudinal direction) will then be defined to be aligned with the 1D element's spatial orientation. For a transversely isotopic material, the solid element's bb- and cc- axes (i.e. local transverse directions) are then easily computed as they lie on a plane orthogonal to the undulating centerline.

Results and Discussion

Figure (4) compares the realistic and idealized virtual microstructures with the experimental microstructures. In the experimental microstructure, the warp yarns appear sinusoidal in shape while the fill yarns appear elliptical in shape. The warp yarns are thicker than the fill yarns and have sharper edges, while the fill yarns are wider than the warp yarns. Note that both the warp and fill yarns in the Kevlar S706 fabric are comprised of the same 600 denier Kevlar KM2 yarns with the same number of fibers within each yarn, and the warp-warp yarn spacing (i.e. yarn span) is the same as the fill-fill yarn spacing.
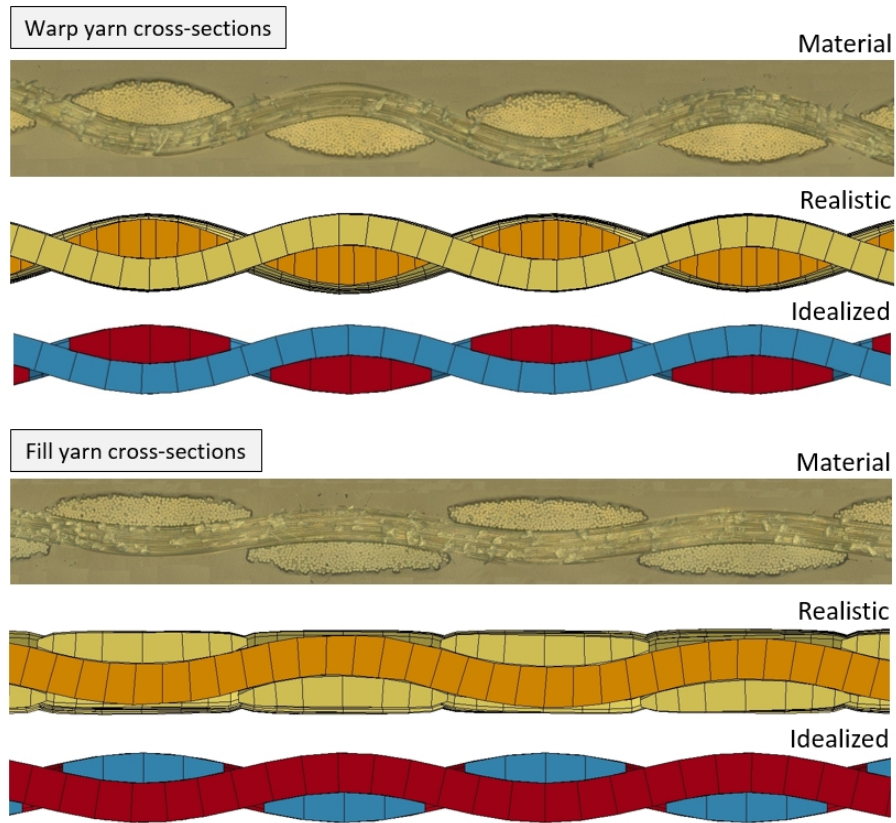
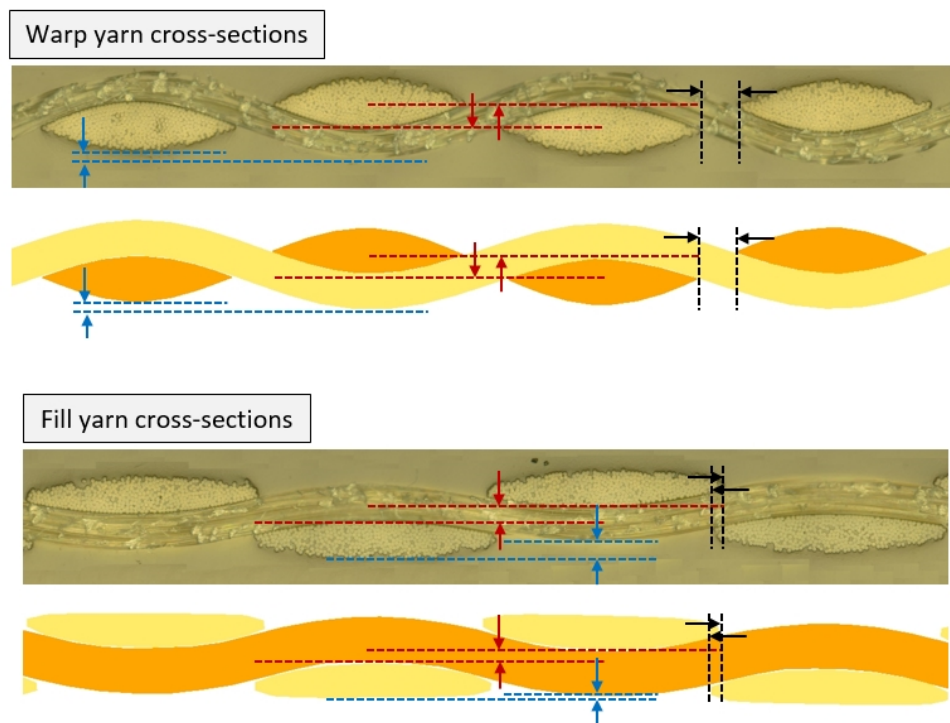**Figure 4. Comparison of the Kevlar S706 fabric experimental and virtual microstructures**
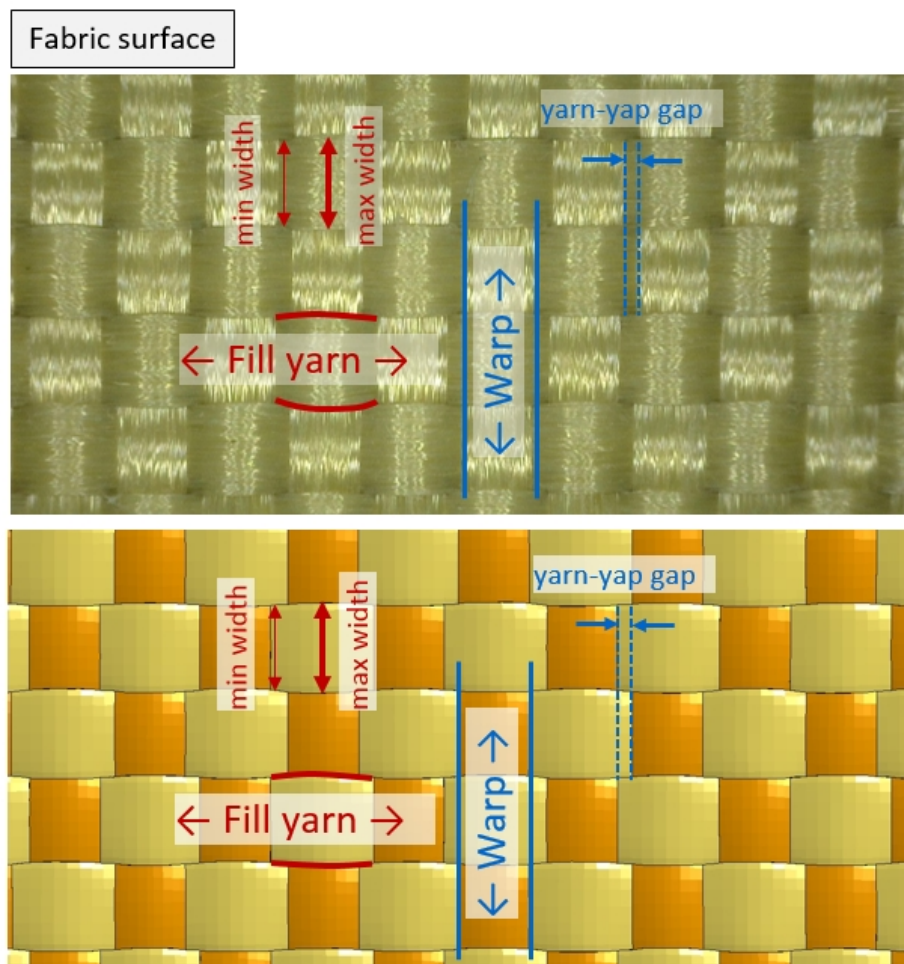

Figure 5. Capturing of intricate Kevlar S706 fabric microstructural features using the thermal growth approach: yarn cross-sections

Thus, the difference in cross-sectional size is a consequence of the manner of fiber packing and distribution within the yarn cross-section, i.e. tighter packing will result in smaller yarn cross-sectional areas. The fill yarn centerlines have a greater degree of undulation or crimp than the warp yarn centerlines. This is a consequence of the manner of weaving the plain-weave fabric on a Jacquard head wherein the warp yarns are held under higher tension than the fill yarns and therefore are 'straighter' or have less undulation. Qualitatively, the realistic virtual microstructure provides an excellent representation of the material microstructure in terms of warp and fill yarn cross-sectional shapes and sizes as seen in Figure (4). Moreover, there is a clear distinction between the warp and fill yarn cross-sections in accordance with the actual material. However in the idealized virtual microstructure, both warp and fill yarn cross-sections appear similar. While the warp yarn cross-sections are reasonably well represented, the assumed sinusoidal yarn cross-sectional shape does not well represent the fill yarn cross-sections as is clearly seen in Figure (4).

Figure 6. Capturing of intricate Kevlar S706 fabric microstructural features using the thermal growth approach: fabric surface

Figures (5) and (6) demonstrate how the realistic virtual microstructure is even able to capture several intricate features of the experimental microstructure. For example, in Figure (5), the crests of the fill yarns are higher than the crests of the warp yarns (*see the blue dotted lines*). There is a horizontal gap between two neighboring warp yarns, whereas there is a horizontal overlap between two neighboring fill yarns (*see the black dotted lines*) which implies the fill yarn widths can exceed the yarn span.
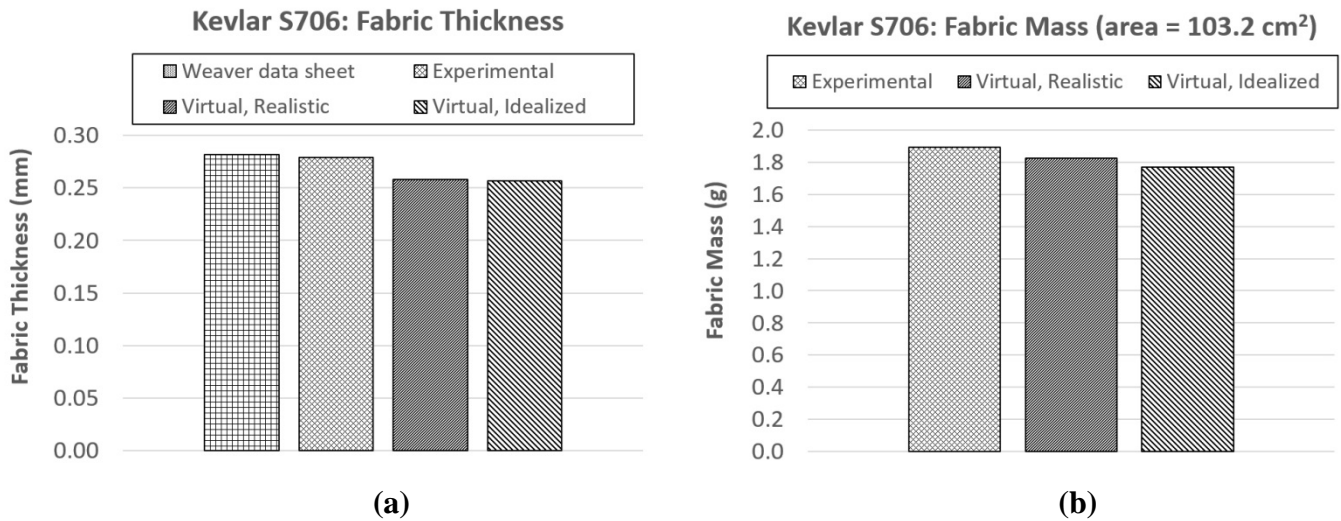
(a)

(b)

Figure 7. Kevlar S706 fabric experimental vs. virtual microstructures (a) fabric thickness (b) fabric mass
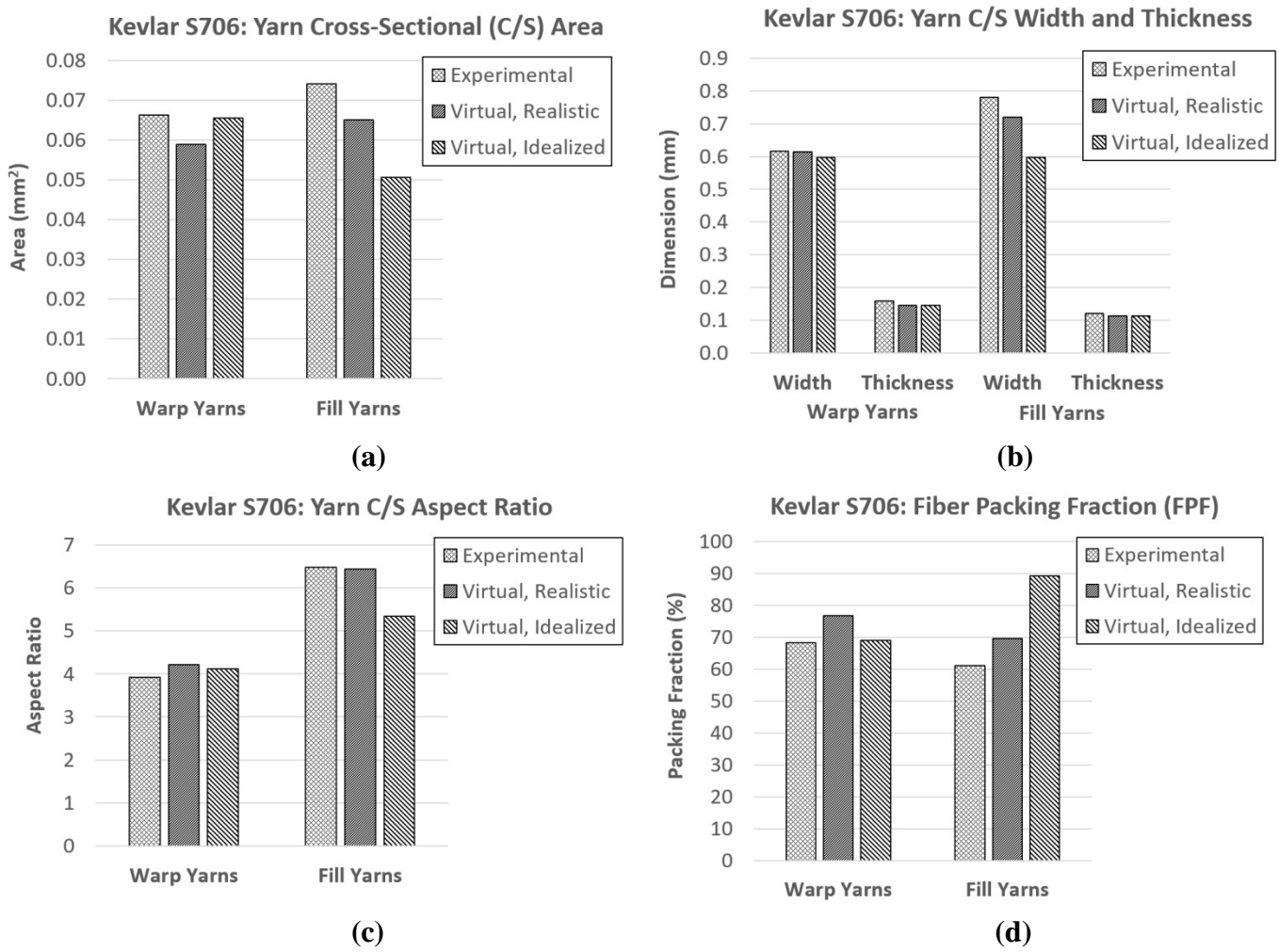

**(a)**

(b)

(c)

(d)

Figure 8. Kevlar S706 fabric experimental vs. virtual microstructures (a) yarn cross-sectional area (b) yarn cross-sectional width and thickness (c) yarn cross-sectional aspect ratio (d) fiber packing fraction

There is a vertical overlap between the contacting regions of two neighboring warp yarns with the interlacing fill yarn, whereas there is a vertical gap between the contacting regions of two neighboring fill yarns with the interlacing warp yarn (*see the red dotted lines*). In Figure (6), the fill yarns tend to spread apart at yarn cross-over locations (*see the red solid outlines*) resulting in a changing yarn width along the fill yarn length. This phenomenon is captured by the realistic virtual microstructure. However, the warp yarns tend to have a constant yarn width along their length (*see the blue solid outlines*) with a constant gap between two warp yarns (*see the blue dotted lines*).

Figures (7) to (9) compare the microstructural dimensions obtained using image analysis between the experimental and virtual microstructures. All reported values correspond to the average of several measurements from the two analyzed micrographs. Some of the dimensions have been measured using both fabric cross-section images (i.e. 'C/S based') and fabric surface images (i.e. 'surface based'). Both virtual microstructures are able to capture the fabric thickness and fabric mass as seen in Figure (7). The idealized virtual microstructure captures the warp yarn cross-sectional area slightly better than the realistic virtual microstructure however it grossly underestimates the fill yarn cross-sectional area as seen in Figure (8a). The reason is apparent in Figure (8b) where the fill yarn width in the idealized virtual microstructure is grossly underestimated, which was previously observed in Figure (4). The other yarn cross-sectional width and thickness dimensions are well predicted by both virtual microstructures. The effect of the underestimated fill yarn width of the idealized virtual microstructure carries over into the yarn cross-sectional aspect ratio and the fiber packing fraction as seen in Figures (8c) and (8d). Figure (9a) compares the gap or spacing between two warp yarns. This parameter was measured using both surface-based images (see Figure 6) and C/S-based images (the difference between the known warp yarn span and the measured warp yarn width). As expected there are slight differences between the two sets of measurements for both the experimental and realistic virtual microstructures. The idealized virtual microstructure utilizes a constant yarn cross-sectional area and shape along its entire length, therefore regardless of the metric used, i.e. surface-based or C/S-based, the warp yarn spacing remained the exact same value. Figure (9b) compares the warp yarn widths from surface-based and C/S-based images, showing excellent agreement between all measurements. Perhaps the most interesting result from this study is seen in Figure (9c) that compares the fill yarn widths from surface-based and C/S-based images. The surface-based measurements allow both the maximum and minimum fill yarn widths to be recorded as was shown in Figure (6). The average of these two min/max measurements is also reported in Figure (9c). For reference, the fill yarn span is also included in Figure (9c) (*see the red dotted line*). For the idealized virtual microstructure, all four values are the exact same for reasons cited earlier, i.e. the yarn cross-sectional area and shape remain constant everywhere. Moreover this value is also grossly underestimated.

(a)

(b)
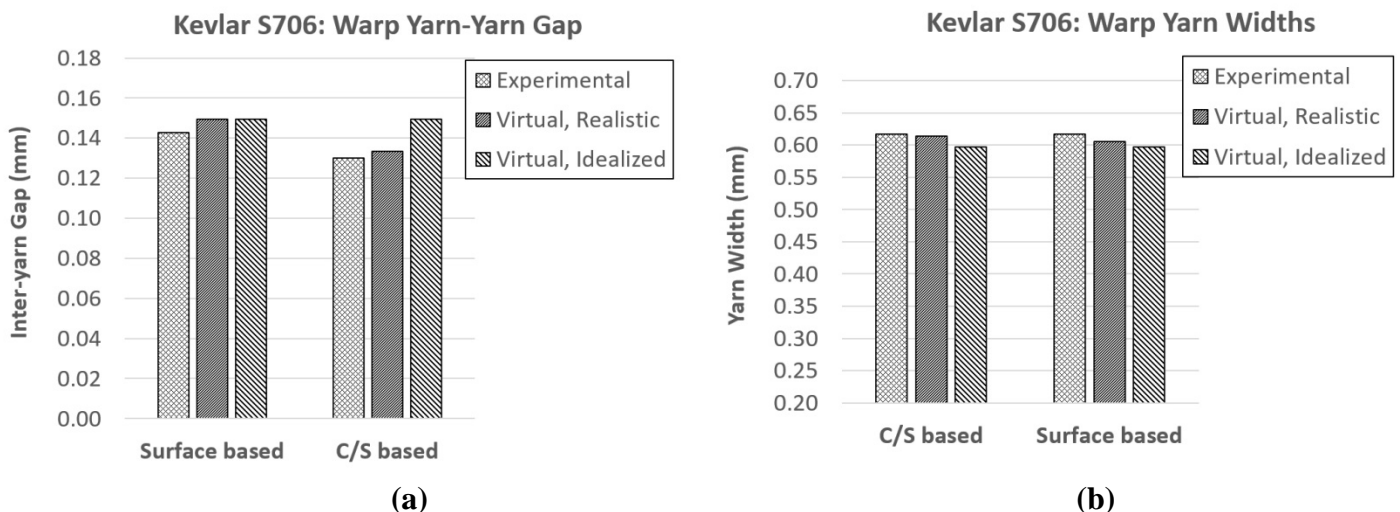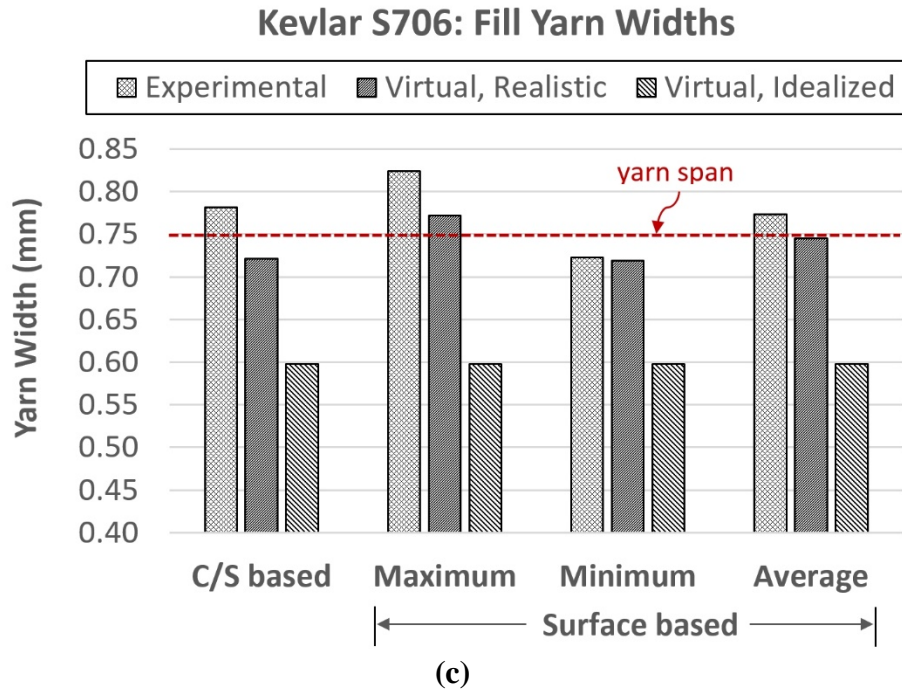
**Figure 9. Kevlar S706 fabric experimental vs. virtual microstructures
(a) warp yarn-yarn gap (b) warp yarn widths (c) fill yarn widths**

Whereas, the realistic virtual microstructure is able to capture variations in the fill yarn width along the fill yarn centerline. The minimum fill yarn width from the realistic virtual microstructure is in excellent agreement with the experimental microstructure. The maximum fill yarn width from the realistic virtual microstructure is lower than the experimental microstructure, however it is still higher than the minimum fill yarn width from the experimental microstructure, and importantly, both the experimental and realistic virtual microstructure show a maximum fill yarn width that exceeds the yarn span. While both the realistic and idealized virtual microstructures captured the warp yarns very well, the idealized virtual microstructure did not capture the fill yarns very well, in particular the fill yarn widths were grossly underestimated. This could be remediated, but only partially, by simply increasing the chosen fill yarn width in the idealized virtual microstructure model which is currently assumed to be some fixed fraction of the yarn span (i.e. 80% in this study). However, the idealized virtual microstructure with the assumed sinusoidal-shaped yarn cross-sections will never be able to capture the maximum observed fill yarn width because its upper bound value is the yarn span; and both the experimental and realistic virtual microstructures clearly showed that the maximum fill yarn width does indeed exceed the yarn span at certain regions along its length. However, this does not mean that the idealized virtual microstructure is inaccurate for finite element simulations. This is because input material properties such as the homogenized yarn density, yarn tensile modulus, and yarn strength are simply consistently adjusted by the respective fiber packing fraction thereby still resulting in accurate composite micromechanics and accurate model predictions, such as those demonstrated in the ballistic impact study of a Kevlar S706 fabric target using the idealized virtual microstructure model [10].

Incorporating Microstructure Stochasticity during the Thermal Growth Process

As mentioned earlier, the starting finite element weave model for the thermal growth process was obtained by sweeping 2D yarn cross-sections along 1D yarn centerlines. These 1D yarn centerlines were idealized, i.e.

they assumed perfectly stacked and parallel yarn columns with no lateral perturbations of the centerline along the yarn length. However these 1D yarn centerlines can themselves have stochasticity initially incorporated in them (for e.g. see [11]), which will have a corresponding probabilistic effect on how the yarns thermally grow against each other. In such a case, it is possible to obtain yarn cross-sectional rotations as well as shearing deformations of the yarn cross-sections in the final virtual microstructure. In this study, during each simulation step, there was one set of applied CTE values to all warp yarns and one set for all fill yarns. There was also one thermal load prescribed to the entire model. In spite of this 'deterministic' application of properties, the resulting virtual microstructure still showed minute variations in the measured microstructure dimensions from yarn to yarn and at different spatial locations of the model, because of the contact algorithms applied between yarn surfaces and the yarn deformations that occurred during the thermal growth. To incorporate actual stochasticity in the resulting virtual microstructure, two strategies can be adopted, which essentially reduce to the manner in which the material properties and loading conditions are applied. The first method is to assign different yarn orthotropic CTE values to each of the individual yarns in the model, that may be randomly scattered or follow some distribution function such as the Normal distribution while keeping the prescribed temperature to the model fixed. The second method is to apply different temperature loadings to the individual yarns of the model while keeping the yarn orthotropic CTE values fixed which will have the same effect. Similarly, the assigned yarn longitudinal and transverse moduli can also have scatter incorporated in them which will have a probabilistic effect on the spatial local yarn deformations during the thermal growth runs. Some trial-and-error or calibration runs may be necessary to determine the extent of scatter required in the input yarn CTE and stiffness properties. These exercises are left to future work.

Other Applications of the Thermal Growth Method for Microstructure Generation

In this paper, a 2D plain weave fabric was presented as an initial exemplar of the thermal growth process to generate realistic virtual microstructures. More generally, this modeling framework can be easily applied to any 2D, 2.5D, and 3D textile architecture for which the 1D centerlines are available. These include weave architectures such as satin harness, angle interlock, layer-to-layer interlock, orthogonal, and stepped orthogonal. Another useful application is to model the stitching thread used to stitch multiple plies of 2D fabric together, such as in Kevlar-based body armor. This is very difficult to generate through analytical or geometry-driven preprocessors, however the mechanics-driven thermal growth method can easily model stitching threads through multiple fabric plies. In addition, volumetric contractions applied along the stitching thread centerlines can also be used to adjust how 'tightly' the plies are stitched or held together. Other applications of the thermal growth process include bi-axial and tri-axial braids, braided structures, and knits. While many knit models assume circular yarn cross-sections, the thermal growth process can be used to precisely capture the changing yarn cross-sections as the loops interlace with each other. For example, Kevlar-based knits are used in soldier groin protection, particularly against ballistic and blast threats. For simulations such as ballistic impact and blast loadings, it is important that the textile finite element model contain properly modeled contact surfaces (i.e. between contacting yarns) because gaps and interpenetrations can result in unwanted, spurious effects during the simulation. By virtue of its underlying paradigm, the thermal growth process automatically results in properly modeled contacting entities (e.g. yarns, threads, etc.). Another interesting application involves generating 3D fiber-level yarn finite element models with stochastic fiber centerlines, stochastic fiber cross-sections, and stochastic fiber packing patterns within the yarn cross-section. Currently, such deterministic 3D fiber-level yarn models [12] assume (a) perfectly circular fibers of the same size, (b) straight and parallel fiber centerlines within the yarn, and (c) ordered fiber packing patterns within the yarn cross-section such as hexagonal close packing (HCP). In reality, the fiber cross-sectional shapes, sizes, packing patterns, and centerlines all demonstrate stochastic variability [12,13] which is important for fiber-level mechanics such as load sharing and frictional interactions between fibers as well as statistical fiber failure which results in a probabilistic yarn failure. Using stochastic 1D fiber centerlines which are relatively easier to generate, the thermal growth process can then be used to generate 3D fibers with stochastic cross-sections, noting that the process of thermal growth with contact definitions between individual fibers will displace the original fiber centerlines to their final realistic configurations. These examples are left as future exercises.

Conclusions

A novel "thermal growth" method has been introduced to generate realistic 3D virtual microstructures of dry fabrics and impregnated composites for various textile architectures. The resulting finite element meshes comprise of high quality elements (either tetrahedral or hexahedral) and smooth, non-penetrating yarn contact surfaces. The thermal growth process is implemented as series of finite element simulations that utilize thermally-induced volumetric expansions and shrinkages coupled with mechanical deformations to grow or form the yarns into their intended and final configurations. The process can result in deterministic or stochastic virtual microstructures depending on how the yarn input material properties and thermal loadings are applied.

We have demonstrated the thermal growth framework for one exemplar case: a plain-weave Kevlar fabric. Detailed validation of the virtual microstructures was provided by comparing them to experimental microstructures. This included ImageJ-based image analysis of the material microstructure characterized using optical microscopy. Another case study pertaining to an angle-interlock C/SiC ceramic matrix composite is described in Nilakantan et al. [7].

The thermal growth process can deal with highly complex and conceptual weave architectures that are not possible to model with commercially available analytical or geometry-driven textile finite element preprocessors. The output geometrical and mesh models serve as the foundation for high-fidelity, predictive, and accurate computational simulations of the behavior of fabrics and textile composites. Having an efficient and general textile model generator is critical to improving the state of the art of composites simulation technology, not just for structural simulations, but also for thermal, permeability, electromagnetic, and multifunctional analyses that require a realistic 3D representation of the underlying weave.

Acknowledgements and Disclaimer

References

[1] Lin H, Brown LP, Long AC. Modelling and Simulating Textile Structures Using TexGen. Advanced Materials Research 2011;331:44-47.

[2] Verpoest I, Lomov SV. Virtual textile composites software Wisetex: integration with micro-mechanical, permeability and structural analysis. Composites Science and Technology 2005;65(15-16):2563-2574.

[3] Wang Y. Digital element approach: a powerful computational tool in textile fabric mechanics. Japan International SAMPE Symposium & Exhibition (JISSE-8), Tokyo, Japan November 18-21, 2003.

[4] Numerical modeling of fracture in textile composites by VTMS/BSAM and RX-FEM. Mollenhauer, D.; Zhou, E.; Iarve, E. 20th International Conference on Composite Materials, Copenhagen, Denmark July 19-24, 2015.

[5] Gowayed Y, Yi L. Mechanical behavior of textile composite materials using a hybrid finite element approach. Polymer Composites 1997;18(3):313-319.

[6] Challa P, Shivakumar KN. mmTEXlam© - A graphical user interfaced design code for laminated textile fabric composites. 19th AIAA Applied Aerodynamics Conference, Anaheim, CA, USA June 2001.

[7] Nilakantan G, Cox B, Sudre O. Generation of realistic stochastic virtual microstructures using a novel thermal growth method for woven fabrics and textile composites. American Society for Composites 32nd Technical Conference, West Lafayette, IN, USA October 22-25, 2017.

[8] Hallquist JO. LS-DYNA Theory Manual. Livermore Software Technology Corporation March 2006.

[9] Nilakantan G, Sudre H. Modeling and analysis tools (DARPA Materials Development for Platforms). National Space & Missile Materials Symposium, Indian Wells, CA, USA June 26-29, 2017.

[10] Nilakantan G. World's first predictive and validated yarn-level FEA modeling of the V0-V100 probabilistic penetration response of fully-clamped Kevlar fabric. American Society for Composites 32nd Technical Conference, West Lafayette, IN, USA October 22-25, 2017.

[11] Blacklock M, Bale H, Begley M, Cox B. Generating virtual textile composite specimens using statistical data from micro-computed tomography: 1D tow representations for the Binary Model. Journal of the Mechanics and Physics of Solids 2012;60:451-70.

[12] Nilakantan G. Filament-level modeling of Kevlar KM2 yarns for ballistic impact studies. Composite Structures 2013;104:1-13.

[13] Recchia S, Zheng JQ, Horner S, Pelegri AA. Multiscale modeling of randomly interwoven fibers for prediction of KM2 Kevlar yarn strength and damage. Acta Mech. 2015 12/01;226(12):4149-58.